Journal of Alloys and Compounds 509 (2011) 8421–8426

Contents lists available at ScienceDirect

Journal of Alloys and Compounds

journal homepage: www.elsevier.com/locate/jallcom

Effect of A site and B site doping on structural, thermal, and dielectric properties of $BiFeO_3$ ceramics

Dinesh Varshney*, Ashwini Kumar, Kavita Verma

School of Physics, Vigyan Bhavan, Devi Ahilya University, Khandwa Road Campus, Indore 452001, India

ARTICLE INFO

Article history:
Received 28 April 2011
Received in revised form 24 May 2011
Accepted 28 May 2011
Available online 13 June 2011

Keywords:
Multiferroics
X-ray diffraction
Rietveld refinement
Raman
Dielectric constant

ABSTRACT

Polycrystalline $Bi_{1-x}Ba_xFe_{1-y}M_yO_3$ (M = Co and Mn; $x = 0.1$, $y = 0.1$) were synthesized by solid-state route method to study the compositional driven structural transformations in multiferroics. Room temperature X-ray diffraction patterns confirmed the formation of perovskite structure. Rietveld-refined crystal structure parameters revealed the existence of rhombohedral *R3c* symmetry for both the samples. The samples were found to be nearly free from any other secondary phases. Raman analysis reveals that Ba atom substitutes Bi site and Mn and Co atom substitutes Fe site into the $BiFeO_3$ with the shifting of phonon modes. The red shift is attributed to Co or Mn doping where as blue shift occurs from Ba doping. The differential scanning calorimetry reveals the corresponding Neel temperature 370 °C and 326 °C for Co and Mn doped samples. Ba and Co substitution with $x = 0.1$ and $y = 0.1$ has not affected the Neel temperature of the parent $BiFeO_3$ as well of Ba and Mn substitution. The variation of frequency dispersion in permittivity and loss pattern due to A-site and B-site substitution in $BiFeO_3$ was observed in the dielectric response curve.

1. Introduction

Recently, ferroelectromagnetic or multiferroics are focused due to inherent ferroelectric properties together with ferromagnetic or ferroelastic properties. In these materials, magneto-electric (ME) effect occurs in which the magnetization is controlled by applied electric field or the electric polarization is controlled by magnetic field [1]. The multiferroism is indeed a subject of intense research as these materials provide a wide range of applications, including data-storage device, spintronics, magnetoelectric sensor devices and multiple-state memories [2].

Currently studied multiferroics includes the rare-earth (RE) manganite $REMnO_3$ or the Bi^{3+}-based perovskites $BiMnO_3$, $BiFeO_3$ or $BiCrO_3$. It is worth to mention that most of the existing single-phase magnetoelectric multiferroics, e.g., $BiMnO_3$, do not exhibit magnetoelectric effect at room temperature. From application point of view the requirement is a material with a large magnetoelectric coupling, however, the magnetoelectric coupling of most of these materials are normally small. Furthermore, it is rather difficult to find a material with a large magnetoelectric effect at room temperature. It is identified that magnetoelectric coupling is usually enhanced around transition temperatures. Hence, it is required to synthesize a material with a large magnetoelectric effect at room temperature to bring T_N or T_C to around room temperature.

$BiFeO_3$ is widely studied due to coupling between ferroelectric and magnetic order at room temperature, causing the possibility of room temperature multiferroic devices. $BiFeO_3$ has a rhombohedrally distorted perovskite structure (space group *R3c*) [3] with chemical formula ABO_3 and Curie temperature ($T_C \sim 830$ °C). The ferroelectricity in $BiFeO_3$ is attributed to the Bi^{3+} $6s^2$ lone pair electrons, where as magnetism is believed to originate from the partially filled d orbital of Fe [4]. It simultaneously shows G-type canted anti-ferromagnetic order below ($T_N = 370$ °C) with a spatially modulated spiral spin structure [5,6]. Even though magnetoelectric coupling could be observed at room temperature it is difficult to observe the ferroelectric loop of bulk $BiFeO_3$ by the magnetic field sweeping.

$BiFeO_3$ could not be exploited for any novel application because of two major reasons; foremost is the weak magnetization as it is antiferromagnetic below T_N, and secondly low resistivity and large loss factor because of oxygen non-stoichiometry. Substitution at Bi or Fe site that helps in minimizing the conductivity and hence the loss factor and enhances the ferroelectric and ferro/antiferromagnetic ordering at room temperature [7–9].

It has been observed that below 10% La doping in $Bi_{1-x}La_xFeO_3$ maintains the rhombohedral structure. However, for 20% and 30% La doping, the structures change to the orthorhombic and tetragonal, respectively. It is noticed that La doping significantly enhances

* Corresponding author. Tel.: +91 731 2467028; fax: +91 731 2465689.
E-mail address: vdinesh33@rediffmail.com (D. Varshney).

0925-8388/$ – see front matter © 2011 Elsevier B.V. All rights reserved.
doi:10.1016/j.jallcom.2011.05.106

the ferromagnetic moment, reduces electric leakage due to the broken cycloid spin structure caused by the changes in the crystalline structure [10]. Furthermore, Ho doping at Bi site in $BiFeO_3$ reduces the leakage current and enhances the ferroelectric switching characteristic while explanatory the stereochemical activity of Bi lone pairs [11,12]. It has been observed that in Sm doped $BiFeO_3$ the spiral spin modulation peculiar to pure $BiFeO_3$ was suppressed in the orthorhombic phase, leading to the weak ferromagnetic properties [13] The Sr doping at Bi-site result in oxygen stoichiometric and with the increase in Sr concentration $SrFeO_3$ phase is accompanied by decrease in magnetization [14]. Similar behavior has also been observed in Ca, Ba doped $BiFeO_3$ samples without any enhancement in magnetization [15].

The Ba doping at Bi site in $BiFeO_3$ enhanced multiferroic properties via enhancing magneto-electric interaction. It has been observed that saturation magnetization increases with increase in Ba doping in $Bi_{1-x}Ba_xFeO_3$ ($x = 0.1$–0.3). Furthermore, the polarization increased with Ba doping up to $x = 0.2$ and a reduction is observed with further increase in Ba doping. This could be attributed to the fact that c/a ratio increases with increase in Ba ions up to $x = 0.2$ and then it decreases considerably [16]. Mn doping at Fe site in $BiFeO_3$ have been studied with an objective that Mn will introduce a mixed valence of Fe (*i.e.*, Fe^{3+} and Fe^{2+}) with a result that Mn does not introduce ferromagnetism. The Mn doping also generates microstructural changes manifested by anisotropic strain broadening, and the average magnetic moment and ordering temperature decreases with increasing Mn concentration [9,17]. On the other hand, magnetization, remanence and coercivity of the La and Co doped samples increases with increasing Co content. In addition to this the dielectric properties is also controlled and led to the reduction of dielectric loss [18]. Thus, A-site doping with biggest ionic radii found to suppress spiral-spin structure, leading to weak ferromagnetism and B-site doping with other transition metal ions increases the spontaneous magnetization with a decrease in ordering temperature.

It is extremely hard to synthesize the single-phase and stoichiometric form of bulk BFO since the temperature stability range of the phase is rather narrow. Also, it is difficult to control oxygen stoichiometry in the sample as impurity phases (*i.e.*, $Bi_{25}FeO_{39}$, Bi_2O_3, $Bi_2Fe_4O_9$, etc.), magnetic defect ions or deviation from the ideal oxygen stoichiometry can always be observed. Literature witnessed that most of the characterizations as X-ray diffraction (XRD), scanning electronic microscopy (SEM), dielectric measurement, electric measurements and magnetic measurements have been performed extensively [19,20]. On the other hand, Raman spectroscopy to study the elementary excitation and their interactions has been less explored in $BiFeO_3$.

In the present paper, we aimed at understanding how the Raman characters of $BiFeO_3$ are affected by excited wavelength of 632.8 nm. We thus report the synthesis $Bi_{0.9}Ba_{0.1}Fe_{0.9}M_{0.1}O_3$ (M = Co, Mn) by solid-state reaction route and study the effect of doping on crystal structure by X-ray diffraction, Raman characters by Raman spectroscopy, dissipation factor from dielectric measurements and Néel temperature from differential scanning calorimetry.

2. Experimental details

The polycrystalline samples with the composition $Bi_{0.9}Ba_{0.1}Fe_{0.9}M_{0.1}O_3$ (M = Co, Mn) were prepared by conventional solid-state route method. High purity analytical grade Bi_2O_3, $BaCO_3$, Fe_2O_3, MnO_2, and Co_3O_4 were used as starting materials. These materials were carefully weighed and stoichiometrically mixed in an agate mortar for 6 h using high purity alcohol as a medium and then calcined at 650 °C for 6 h. The resultant powders were again ground and pressed into 10 mm diameter and 2 mm thick pellets. Finally the pellets were sintered at 830 °C for 3 h resulting in good densification.

The samples were characterized by means of X-ray diffraction (XRD), Raman spectroscopy, and differential scanning calorimetry at room temperature. The XRD measurements were carried out with CuKα (1.54 Å) radiation using a 18 kW Rigaku powder diffractometer equipped with a rotating anode scanning (0.02 step in 2θ) over the angular range 10–90° at room temperature generating X-ray by 40 kV and 100 mA power settings and analyzed with Rietveld refinement program.

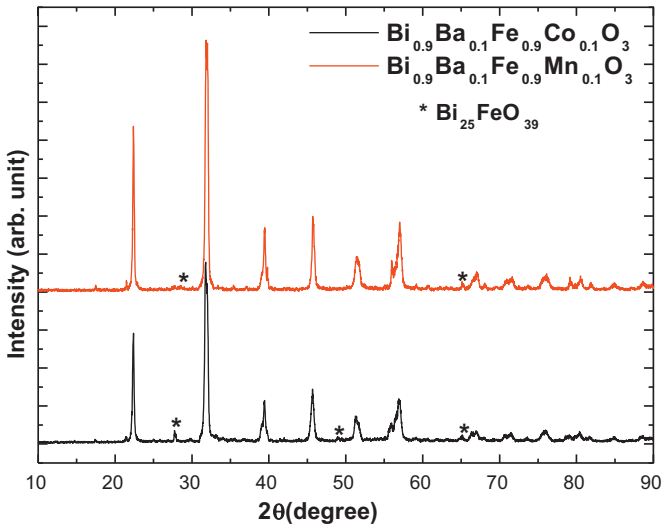

Fig. 1. X-ray diffraction (XRD) pattern for $Bi_{0.9}Ba_{0.1}Fe_{0.9}M_{0.1}O_3$ (M = Co, Mn) samples.

The Raman equipment was a Jobin-Yovn Horiba Labram (System HR800) consisting of a single spectrograph (0.25 m focal length) containing a holographic grating filter (1800 grooves mm^{-1}), and a Peltier-cooled CCD detector (1024 × 256 pixels of 26 μm). The spectra were excited with 632.8 nm radiation (1.95 eV) from a 19 mW air-cooled He–Ne laser (Max Laser power: 19 mW) and the laser beam was focused on the sample by a 50× lens to give a spot size of 1 μm; the resolution was better than 2 cm^{-1}. The laser power was always kept on 5 mW at the sample, to avoid sample degradation, except in the laser power dependence experiments. After each spectrum had been recorded, a careful visual inspection was performed using white light illumination on the microscope stage in order to detect any change that could have been caused by the laser.

The modulated DSC measurement was carried out on TA Instruments Model 2910 MDSC equipment from temperature 200 °C to 500 °C in inert (N_2) atmosphere with a heating rate of 5 °C/min and ±0.75 °C modulations per 60 s. The samples were thinned downed to 1.0 mm thick, and high temperature silver paste was applied on their two major surfaces as electrodes for dielectric measurements. Dielectric measurements were carried out in the frequency range (100 Hz to 1 MHz) using an impedance analyzer (HP 4194 A).

3. Results and discussion

3.1. Structural analysis

The X-ray powder diffraction pattern of $Bi_{0.9}Ba_{0.1}Fe_{0.9}M_{0.1}O_3$ (M = Co, Mn) samples at room temperature is illustrated in Fig. 1. For both the compounds, a small amount of $Bi_{25}FeO_{39}$ impurity phase was detected (marked by *) that is neither ferroelectric [21], nor magnetically ordered [22]. The XRD pattern of both the samples revealed the formation of nearly single-phase rhombohedral structure that can be described in hexagonal frame of reference with *R*3*c* space group. The structural parameters were analyzed by the Rietveld refinement using the Fullprof program [23]. The program allowed us to reproduce all observed reflections and gave all identical reliability factors.

The Rietveld refinement result of $Bi_{0.9}Ba_{0.1}Fe_{0.9}M_{0.1}O_3$ (M = Co, Mn) samples is documented in Fig. 2. It is noticed that the simulated XRD pattern agrees well with the measured data with no structural phase transition from rhombohedral to any other phase as it has been reported earlier that Ba and Mn substitution with ($x \leq 0.4$) has not affected the crystalline structure of the parent compound BFO, which is important for the FE properties of the compounds [24]. It is worth to comment that Jayakumar and researchers have synthesized $Bi_{1-x}Ba_xFe_{1-y}Mn_yO_3$ ($x = 0.0$ and 0.1; $y = 0.0$ and 0.2)

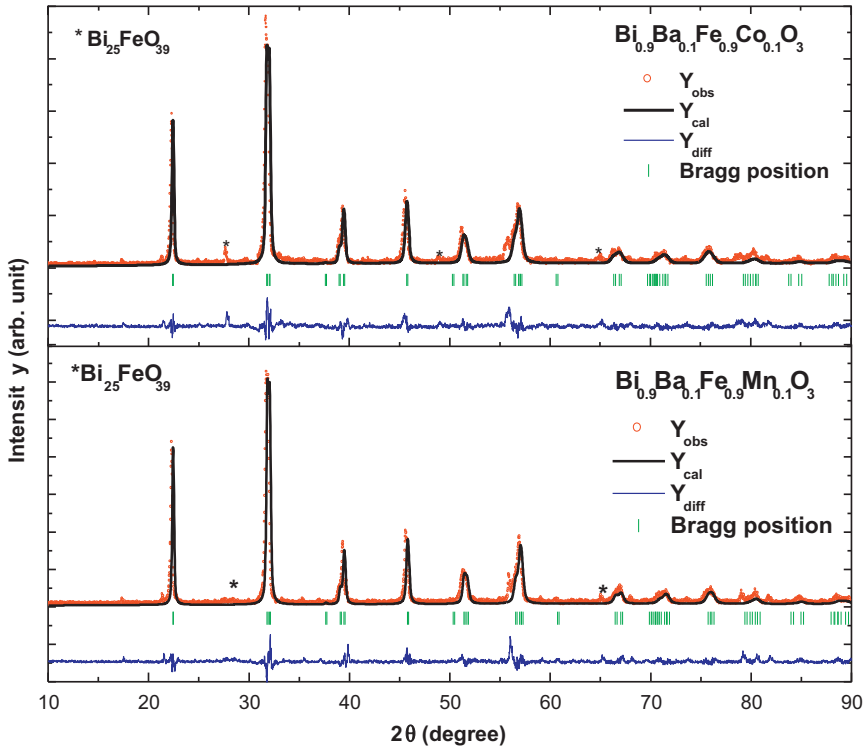

Fig. 2. The Rietveld refinement using Fullprof Program for $Bi_{0.9}Ba_{0.1}Fe_{0.9}M_{0.1}O_3$ (M = Co, Mn) samples.

compositions by the pyrolysis of xerogel precursors [25]. The powder X-ray diffraction XRD patterns were analyzed by Rietveld refinement of using FULLPROF 2000. Structural studies by X-ray diffraction and transmission electron microscopy show a tetragonal lattice for Ba substituted $BiFeO_3$ and a rhombohedral lattice for Mn substituted $BiFeO_3$. The analyses of XRD data with a biphasic model leads to coexistence of distorted rhombohedral and tetragonal phases is observed in Ba and Mn codoped $BiFeO_3$. However, we have analyzed the XRD data with single-phase model to get only distorted rhombohedral phase.

The calculated parameters of $Bi_{0.9}Ba_{0.1}Fe_{0.9}M_{0.1}O_3$ (M = Co, Mn) after refinement in *R*3*c* space group are listed in Table 1. We summarized structural parameters for both samples and also identify the residuals for the weighted pattern Rwp, the pattern Rp, Braggs factor R_{Bragg}, structure factor R_F, and goodness of fit χ^2. Refined occupation cationic positions suggest that both the structures have completely different compositions corresponding to the chemical formula of the compound.

3.2. Optical analysis

Fig. 3(a and b) represents the Raman spectra of $Bi_{0.9}Ba_{0.1}Fe_{0.9}M_{0.1}O_3$ (M = Co, Mn) at 300 K with excitation wavelength of 632.8 nm, respectively. On decomposing the fitted curves into individual Lorentzian components, the peak position of each component, *i.e.*, the natural frequency of each Raman active mode, was obtained. The resolved Raman modes of the samples marked by pointing arrows can be indexed to the modes of pure $BiFeO_3$. The Raman modes of pure $BiFeO_3$ [26] and dependence of mode position on substitution with Ba at A-site and Co and Mn at B-site are summarized in Table 2. We may add that it is difficult to obtain $BiFeO_3$ as a pure single phase. Additional (secondary) phases usually exist in this material and it causes that its properties are worse. It is known that $BiFeO_3$ belongs to distorted rhombohedral structure with *R*3*c* space group. Ten atoms in the unit cell of this structure yields 18 optical phonon modes $\Gamma_{opt} = 4A_1 + 5A_2 + 9E$. According to group theory ($4A_1 + 9E$) are 13 Raman active modes $\Gamma_{Raman} = 4A_1 + 9E$, whereas $5A_2$ are Raman inactive modes.

The A_1 modes are associated with Fe ions and E modes are associated with Bi ions [27,28]. The A_1 modes of doped samples shows relatively slow shift towards the lower wave number as compared to pure $BiFeO_3$ with sudden disappearance of some modes. On the other hand E modes of $Bi_{0.9}Ba_{0.1}Fe_{0.9}M_{0.1}O_3$ (M = Co, Mn) are shifted towards higher frequency side. The modes E-2, E-8 and E-9 show the greater shift to higher frequency as compared to other E modes.

Table 1
Structural parameter for $Bi_{0.9}Ba_{0.1}Fe_{0.9}M_{0.1}O_3$ (M = Co, Mn) obtained by Rietveld refinement of the XRD patterns at room temperature.

Material	Crystal structure	Lattice parameters (Å)	Atomic positions and volume	*R* factors
BBFCO	Rhombohedral (*R*3*c*)	*a* = 5.5880 *b* = 5.5880 *c* = 13.846	Bi/Ba (0, 0, 0) Fe/Co (0, 0, 0.2630) O (0.4590, 0.2577, 0.9612) Volume = 374.55 Å^3	$\chi^2 = 4.75$ $R_{Bragg} = 10.6$ $R_F = 9.34$
BBFMO	Rhombohedral (*R*3*c*)	*a* = 5.5815 *b* = 5.5815 *c* = 13.818	Bi/Ba (0, 0, 0) Fe/Mn (0, 0, 0.2350) O (0.4437, 0.0255, 0.9617) Volume = 372.82 Å^3	$\chi^2 = 5.88$ $R_{Bragg} = 8.59$ $R_F = 8.02$

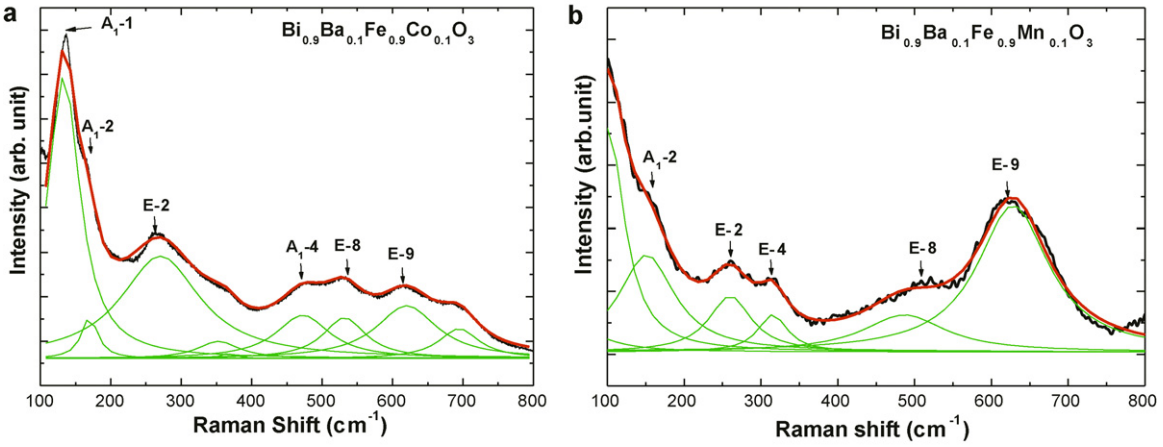

Fig. 3. (a) Raman Spectra for $Bi_{0.9}Ba_{0.1}Fe_{0.9}Co_{0.1}O_3$ at room temperature with excitation wavelength of 632.8 nm. (b) Raman Spectra for $Bi_{0.9}Ba_{0.1}Fe_{0.9}Mn_{0.1}O_3$ at room temperature with excitation wavelength of 632.8 nm.

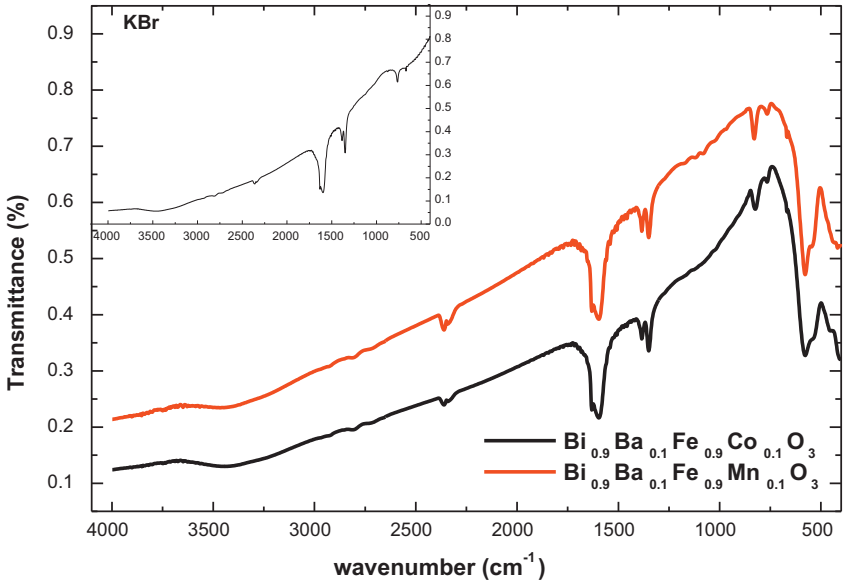

Fig. 4. Room temperature FTIR spectra for $Bi_{0.9}Ba_{0.1}Fe_{0.9}M_{0.1}O_3$ (M = Co, Mn) samples.

The above changes are attributed to the change of Bi–O covalent bond with Ba substitution at Bi site as well Co or Mn doping at Fe site. The shifting of modes at lower frequency side is mainly due to the substitution of Fe with Co or Mn, which causes the structural distortion at Fe-site, fewer changes can be observed on Co doping as compared to Mn substitution. The higher frequency shift may be due to the substitution of light mass Ba^{2+} ion for Bi^{3+} which reduces the average mass of the A-site, since the frequencies of the Raman modes are dependent on force constant and ionic mass so the normal modes related to Bi–O bond shift towards the higher frequency side.

Fourier transform infrared spectroscopy (FTIR) is one of the preferred methods of infrared spectroscopy. The transmission IR spectra of $Bi_{0.9}Ba_{0.1}Fe_{0.9}M_{0.1}O_3$ (M = Co, Mn) samples in the wave number range of 4000–400 cm^{-1} are shown in Fig. 4. The band around 577 cm^{-1} corresponds to Fe–O stretching vibration, present in the FeO_6 octahedral unit consistent with the earlier report [29]. The BiO_6 octahedral structure also exhibits absorption peak at about 525 cm^{-1} which is consistent with the previous measurement on parent $BiFeO_3$ (400–600 cm^{-1}) [30]. The broad nature of the observed vibration band at about 577 cm^{-1} is attributed to the occurrence of absorption peak of both iron oxide and bismuth oxide

Table 2
Raman modes of $BiFeO_3$, $Bi_{0.9}Ba_{0.1}Fe_{0.9}M_{0.1}O_3$ (M = Co, Mn) compounds.

Materials	Number of assigned modes (cm^{-1})											
	A_1-1	A_1-2	A_1-3	E-2	E-3	E-4	E-5	A_1-4	E-6	E-7	E-8	E-9
$BiFeO_3$ [26]	139	172	217	262	275	307	345	470	369	429	521	613
BBFCO	135.07	163.68	–	262.63	–	–	346.11	471.17	–	–	529.51	619.88
BBFMO	–	162.40	–	261.55	–	313		–	–	–	521.39	625.70

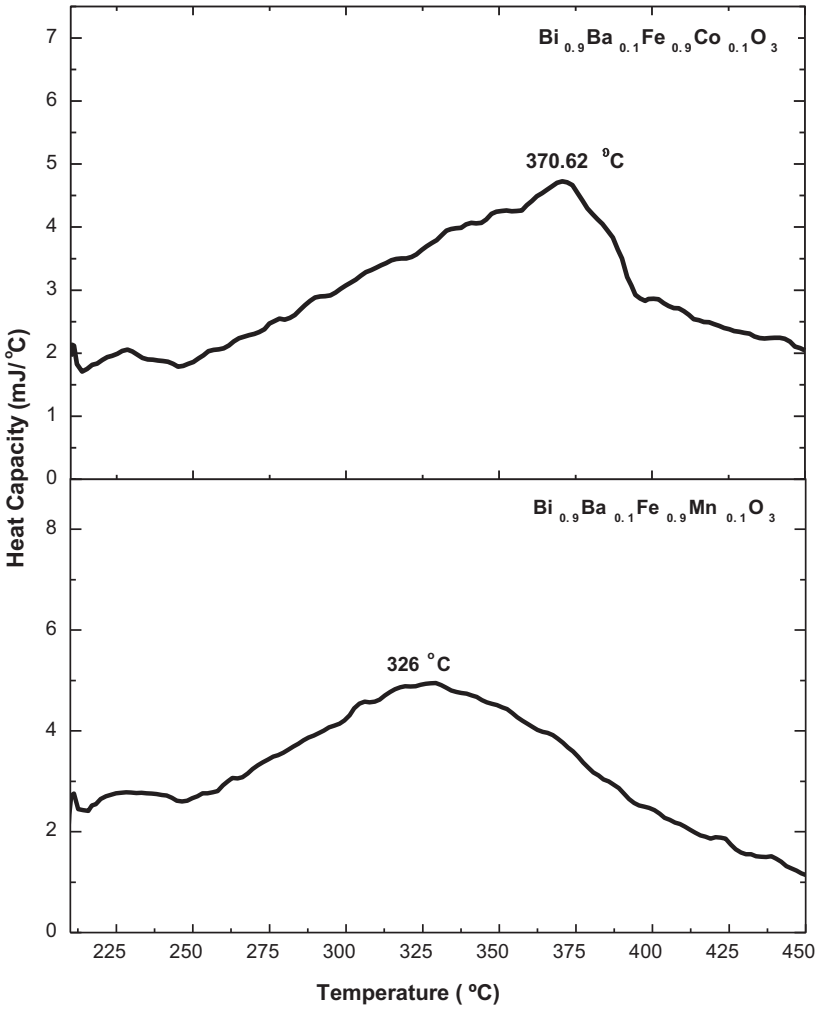

Fig. 5. DSC curve for $Bi_{0.9}Ba_{0.1}Fe_{0.9}M_{0.1}O_3$ (M = Co, Mn) samples.

at nearly same wave number. Furthermore, the observed absorption bands at 2354, 1593, 1348 cm^{-1} are of KBr powder (shown in inset of Fig. 4).

3.3. Thermal analysis

The results of DSC (differential scanning calorimetry) measurements are illustrated in Fig. 5 for both prepared samples in the temperature range of 200–450 °C. For the sake of clarity a base line is subtracted from the data and the resulting data are plotted. It is expected that A-site doping is responsible for the ferroelectric nature and B-site substitution causes for the magnetic ordering of BFO [31]. The transition revealed by the plots is magnetic transitions from antiferromagnetic to paramagnetic. The value of magnetic transition temperature T_N obtained at 370 °C (643 K) for $Bi_{0.9}Ba_{0.1}Fe_{0.9}Co_{0.1}O_3$ matches well with the reported value of pure BFO [32], whereas with Mn doping T_N decreases towards the room temperature and found to be at 325 °C (598 K). The reduction of T_N to near room temperature with Mn doping is used to give large magneto-electric effects at room temperature. The ferroelectric to paraelectric transition could not be observed due to the limitations of the instrument as this transition is expected to be above 800 °C.

3.4. Dielectric analysis

The room temperature dielectric constant (ε') and dielectric loss ($\tan\delta$) for both the samples as a function of frequency is illustrated in Fig. 6. It can be seen from the figure that $Bi_{0.9}Ba_{0.1}Fe_{0.9}M_{0.1}O_3$ (M = Co, Mn) shows decreasing trend in ε' and $\tan\delta$ with increasing frequency from 100 Hz to 1 MHz. We have obtained a value of about 47 and 72 for ε' at room temperature and at about 1 MHz for

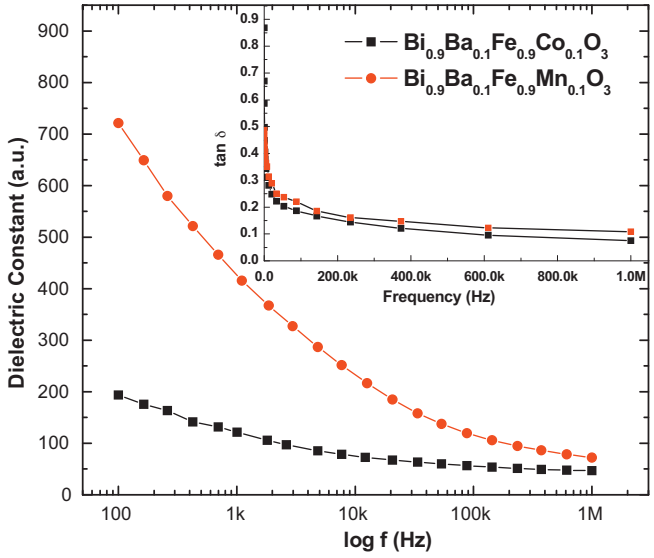

Fig. 6. Variation of dielectric constant and dielectric loss (in inset) with frequency of $Bi_{0.9}Ba_{0.1}Fe_{0.9}M_{0.1}O_3$ (M = Co, Mn) at room temperature.

the bulk $Bi_{0.9}Ba_{0.1}Fe_{0.9}M_{0.1}O_3$ (M = Co, Mn) samples, respectively. The above is comparable with the previous measurements on bulk $Ni_{0.5}Zn_{0.5}Fe_2O_4$ ferrites (~50) [33], pure $BiFeO_3$ (~45.5) and $Bi_{0.9}Nd_{0.1}FeO_3$ (~75) ceramics [34,35]. Some authors have reported high value of dielectric constant in $BiFeO_3$ (~250), $Bi_{0.825}Tb_{0.075}La_{0.1}FeO_3$ (~450) and thin films (~378) [36–38]. Furthermore, $Bi_{0.9}Ba_{0.1}Fe_{0.9}M_{0.1}O_3$ (M = Co, Mn) samples possess larger $\tan\delta$ value of about 0.1 (0.074) (<10%) in the whole frequency range of measurement when compared with the $BiFeO_3$ samples [39]. It is inferred that the dielectric constant (ε') have higher values and dielectric loss ($\tan\delta$) have smaller value for Mn substituted sample.

On comparing dielectric constant (ε') of the pristine $BiFeO_3$ with both the doped samples, we find a lower value of dielectric constant. This is consistent with the increase in the band gap as wide band gap materials are expected to have a lower dielectric constant following the inverse proportionality relation [40,41]. Further, an interesting trend emerges if we look at the ε' values of the doped BFO samples. It can be noticed that the dielectric constant decreases as the ionic radius of the dopant increases. This is in agreement with previous studies where a similar correlation between the ionic radii and the dielectric constant was obtained [42,43].

Usually, the dipolar, electronic, ionic, and interfacial polarizations contributes to the dielectric constant of any material. At low frequencies, it is the dipolar and interfacial polarizations are effective to the dielectric constant. However, at higher frequencies the electronic polarization is effective and dipolar contribution becomes insignificant. The decrease in dielectric constant with increased frequency could be explained on the basis of dipole relaxation phenomenon. It is depicted from Fig. 6 that at lower frequency the dipoles in bulk $Bi_{0.9}Ba_{0.1}Fe_{0.9}M_{0.1}O_3$ (M = Co, Mn) sample are able to follow the frequency of the applied field but at higher frequency there is a weak dependence of ε' on frequency. Henceforth, the ferroelectric domain contributes to the behavior of dielectric constant rather than dipole.

4. Conclusions

Polycrystalline samples of $Bi_{0.9}Ba_{0.1}Fe_{0.9}M_{0.1}O_3$ (M = Co, Mn) were successfully prepared by solid-state route method. The effect of doping in the BFO compound on its structural, dielectric behavior has been studied. X-ray diffraction confirms the formation of single phase with some impurity of about 1–2%. Both the samples fitted with Rietveld refinement using Fullprof Program revealed the existence of rhombohedral structure with space group *R*3*c*. Evolution of Raman spectra reveals the active phonon modes for both the samples and shifting of phonon modes because of doping concentration. A reduction of the Neel temperature has been observed in the Mn doped sample in comparison the Co-doped one. Larger dielectric constant and small loss is observed for Mn-doped sample as compared to the Co doped sample at high frequency (1 MHz).

Acknowledgements

The authors wish to thank UGC-DAE CSR, Indore for providing characterization facilities and financial assistance. We thank Dr. Sunil Verma for his help in carrying out dielectric measurements.

References

[1] W. Prellier, M.P. Singh, P. Murugavel, J. Phys.: Condens. Matter 17 (2005) R803.
[2] G. Catalan, J.F. Scott, Adv. Mater. 21 (2009) 2463.
[3] J.B. Neaton, C. Ederer, U.V. Waghmare, N.A. Spaldin, K.M. Rabe, Phys. Rev. B 71 (2005) 014113.
[4] R. Seshadri, N.A. Hill, Chem. Mater. 13 (2001) 2892.
[5] I. Sosnowska, T.P. Neumair, J. Phys. C: Solid State Phys. 15 (1982) 4835.
[6] W. Kaczmarek, Z. Pajak, Solid State Commun. 17 (1975) 807.
[7] X. Qi, J. Dho, R. Tomov, Appl. Phys. Lett. 86 (2005) 062903.
[8] Y.K. Jun, W.K. Moon, C.-M. Chang, H.-S. Kim, Hyun, S. Ryu, J.W. Kim, K.H. Kim, S.-H. Hong, Solid State Commun. 135 (2005) 133.
[9] V.R. Palkar, D.C. Kundaliya, J. Appl. Phys. 93 (2003) 4337.
[10] Z.X. Cheng, A.H. Li, X.L. Wang, S.X. Dou, K. Ozawa, H. Kimura, S.J. Zhang, T.R. Shrout, J. Appl. Phys. 103 (2008) 07E507.
[11] N.V. Minh, N.G. Quan, J. Alloys Compd. 509 (2011) 2663.
[12] N. Jeon, D. Rout, I.W. Kim, S.-J.L. Kang, Appl. Phys. Lett. 98 (2011) 072901.
[13] V.A. Khomchenko, J.A. Paixão, B.F.O. Costa, D.V. Karpinsky, A.L. Kholkin, I.O. Troyanchuk, V.V. Shvartsman, P. Borisov, W. Kleemann, Cryst. Res. Technol. 46 (3) (2011) 238.
[14] J. Li, Y. Duan, J. Alloys Compd. 315 (2001) 259.
[15] V.A. Khomchenko, D.A. Kiselov, Mater. Lett. 62 (2008) 1927.
[16] A. Gautam, V.S. Rangra, Cryst. Res. Technol. 45 (2010) 953.
[17] I. Sosnowska, Appl. Phys. A 74 (2002) S1042.
[18] F.Z. Qian, J.S. Jiang, D.M. Jiang, C.M. Wang, W.G. Zhang, J. Magn. Magn. Mater. 322 (2010) 3127.
[19] R. Haumont, J. Kreisel, P. Bouvier, F. Hippert, Phys. Rev. B 73 (2006) 132101.
[20] M.K. Singh, H.M. Jang, S. Ryu, M.H. Jo, Appl. Phys. Lett. 88 (2006) 042907.
[21] P.S. Halasyamani, K.R. Poeppelmeier, Chem. Mater. 10 (1998) 2753.
[22] D. Lebeugle, D. Colson, A. Forget, M. Viret, P. Bonville, J.F. Marucco, S. Fusil, Phys. Rev. B 76 (2007) 024116.
[23] J. Rodríguez-Carvajal, Physica B 192 (1993) 55.
[24] L.H. Yin, W.H. Song, X.L. Jiao, W.B. Wu, X.B. Zhu, Z.R. Yang, J.M. Dai, R.L. Zhang, Y.P. Sun, J. Phys. D: Appl. Phys. 42 (2009) 205402.
[25] O.D. Jayakumar, S.N. Achary, K.G. Girija, A.K. Tyagi, C. Sudakar, G. Lawes, R. Naik, J. Nisar, X. Peng, R. Ahuja, Appl. Phys. Lett. 96 (2010) 032903.
[26] Y. Yang, J.Y. Sun, K. Zhu, Y.L. Liu, J. Chen, X.R. Xing, Physica B 404 (2009) 171.
[27] P. Kharel, S. Talebi, B. Ramachandran, A. Dixit, V.M. Naik, M.B. Sahana, C. Sudakar, R. Naik, M.S.R. Rao, G. Lawes, J. Phys.: Condens. Matter 21 (2009) 036001.
[28] S. Yasui, H. Uchida, H. Nakaki, K. Nishida, H. Funakubo, S. Koda, Appl. Phys. Lett. 91 (2007) 022906.
[29] G.V.S. Rao, C.N.R. Rao, Appl. Spectrosc. 24 (1970) 436.
[30] K.K. Som, S. Molla, K. Bose, B.K. Chaudhury, Phys. Rev. B 45 (1992) 1655.
[31] D.I. Khomskii, J. Magn. Magn. Mater. 306 (2006) 1.
[32] G.A. Smollenskii, V.M. Yudin, Sov. Phys. JETP 16 (1963) 622.
[33] N. Sivakumar, A. Narayanasamy, N. Ponpandian, G. Govindaraj, J. Appl. Phys. 101 (2007) 084116.
[34] B. Bhushan, A. Basumallick, S.K. Bandopadhyay, N.Y. Vasanthacharya, D. Das, J. Phys. D. Appl. Phys. 42 (2009) 065004.
[35] R.K. Mishra, K. Dillip, R.N.P. Pradhan, A. Choudhary, Banerjee, J. Magn. Magn. Mater. 320 (2008) 2602.
[36] M. Kumar, K.L. Yadav, J. Appl. Phys. 100 (2006) 074111.
[37] M. Li, M. Ning, Y. Ma, Q. Wu, C.K. Ong, J. Phys. D: Appl. Phys. 40 (2007) 1603.
[38] V.R. Palkar, D.C. Kundaliya, S.K. Malik, S. Bhattacharya, Phys. Rev. B 69 (2004) 212102.
[39] G.L. Yuan, S.W. Or, J. Appl. Phys. 100 (2006) 024109.
[40] P.W. Peacock, J. Robertson, J. Appl. Phys. 92 (2002) 4712.
[41] L.K. Pan, Y.K. Ee, C.Q. Sun, G.Q. Yu, Q.Y. Zhang, B.K. Tay, J. Vac. Sci. Technol. B 22 (2004) 583.
[42] X. Chou, J. Zhai, H. Jiang, X. Yao, J. Appl. Phys. 102 (2007) 084106.
[43] K.C.J. Raju, V. Sivasubramanian, R. Pragasam, B. Viswanathan, V.R.K. Murthy, J. Appl. Phys. 74 (1993) 1968.